SUPPORTING INFORMATION FOR: 'Strength of bacterial adhesion on nanostructured surfaces quantified by substrate morphometry'

Christian Spengler,[a] Friederike Nolle,[a] Johannes Mischo,[a] Thomas Faidt,[a] Samuel Grandthyll,[a] Nicolas Thewes,[a] Marcus Koch,[b] Frank Müller,[a] Markus Bischoff,[c] Michael A. Klatt,[d‡] and Karin Jacobs[a]

[a] Department of Experimental Physics, Saarland University, Campus E2 9, 66123 Saarbrücken, Germany. Fax: +49 (0)681 302 71700; Tel: +49 (0)681 302 71777; E-mail: k.jacobs@physik.uni-saarland.de
[b] INM – Leibniz Institute for New Materials, Campus D2 2, 66123 Saarbrücken, Germany.
[c] Institute of Medical Microbiology and Hygiene, Saarland University, 66421 Homburg/Saar, Germany.
[d] Institute of Stochastics, Karlsruhe Institute of Technology, 76131 Karlsruhe, Germany.
‡ Present address: Department of Physics, Princeton University, Jadwin Hall, Princeton, NJ 08544-0001, USA

XPS Spectrum of a Nanostructured Silicon Surface

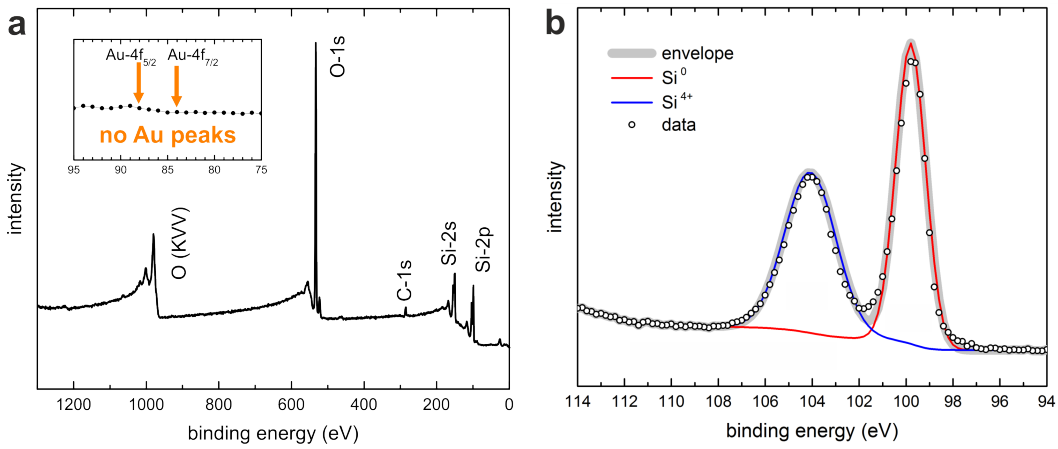

Fig. S1 a) Survey spectrum of a nanostructured surface after cleaning with aqua regia: since there are no Au peaks detectable at energies of about 84 eV and 88 eV (see inset), the gold layer was completely removed by the acid. b) XPS Si-2p data (open circles) of a nanostructured surface (270 s in fluoric acid). The Si^0 line is shown in red (please note that the Si-2p spin orbit splitting is not resolved) and the Si^{4+} line is shown in blue. The ratio of their intensities is used to calculate the oxide layer thickness [1].

Figure S1 shows the XPS data of the Si-2p core level of a (exemplary) nanostructured substrate with both peaks assigned to Si^0 contributions from the bulk and Si^{4+} contributions from the oxide layer. When comparing the intensities of both contributions it is straightforward to estimate the thickness of the oxide layer to be 3.2–4.0 nm. However, it has to be noted that these values have to be considered as an upper limit, since the Si^{4+} contribution is overestimated in the experiment on a nanostructured surface. Due to the high surface sensitivity in XPS, only a thickness of about 1–2 nm is probed and the surface sensitivity increases with increasing the polar angle (i. e. the angle between the surface normal and the direction of the emission of the photoelectrons). For a nanostructured surface, the surface normals of local surface areas

are distributed over a wide range (if compared to a smooth Si wafer) and, therefore, a large part of the overall surface is probed with enhanced surface sensitivity, causing an increased Si^{4+} contribution.

As a consequence, the thickness of the oxide layer of about 3.2–4.0 nm, as probed in experiments on a nanostructured surface, does not really differ from the thickness of about 1.7 nm[1], as probed in experiments on a smooth Si wafer and it is not expected that bacterial adhesion is much affected by the difference in the thickness of the oxide layer[2].

Quality of the Silanization

Table S1 shows water contact angles and hysteresis on the silanized nanostructured surfaces. Compared to the smooth samples (where we know from previous experiments that the silane monolayer is dense and homogeneous[3]), on all nanostructured surfaces, the advancing contact angle as well as the contact angle hysteresis increases. This is in accordance with the literature for structured hydrophobic surfaces[3,4].

Table S1 Advancing water contact angle and hysteresis for all surfaces. The numbers in brackets give the error from three measurements each.

RMS roughness	0.1 nm	7 nm	24 nm	35 nm
Advancing CA	111(1) °	154(2) °	153(3) °	158(2) °
Hysteresis	4(2) °	43(3) °	32(1) °	21(2) °

In addition, the nanostructured surfaces were scanned under water with a hydrophobized AFM tip ('Scanasyst-fluid+' by Bruker) in quantitative nanomechanical mapping (QNM) mode. Fig. S2 shows an overlay of the 3D structure of the topography and the adhesion force between tip and surface for a silanized silicon surface with 7 nm RMS roughness and a PDMS surface that was produced by mold casting the silicon substrate (see page 9 for more details). For both samples, the images are very similar in absolute values of adhesion as well as in the distribution of larger and weaker adhesion sites: significant adhesion (> 1 nN) is visible on every point of the surfaces. Adhesion on both samples is the strongest in the valleys of the surfaces for geometrical reasons, i. e. due to the enlarged interaction area between tip and valley[5]. Since the PDMS substrate has a homogeneous surface chemistry, one would expect a patchy adhesion response of the silanized sample (either around the valleys or around the tips or shoulders) if the silanization was not homogeneous. Hence, we deduce from both experiments (contact angle and adhesion measurements) that the silanization is homogeneous.

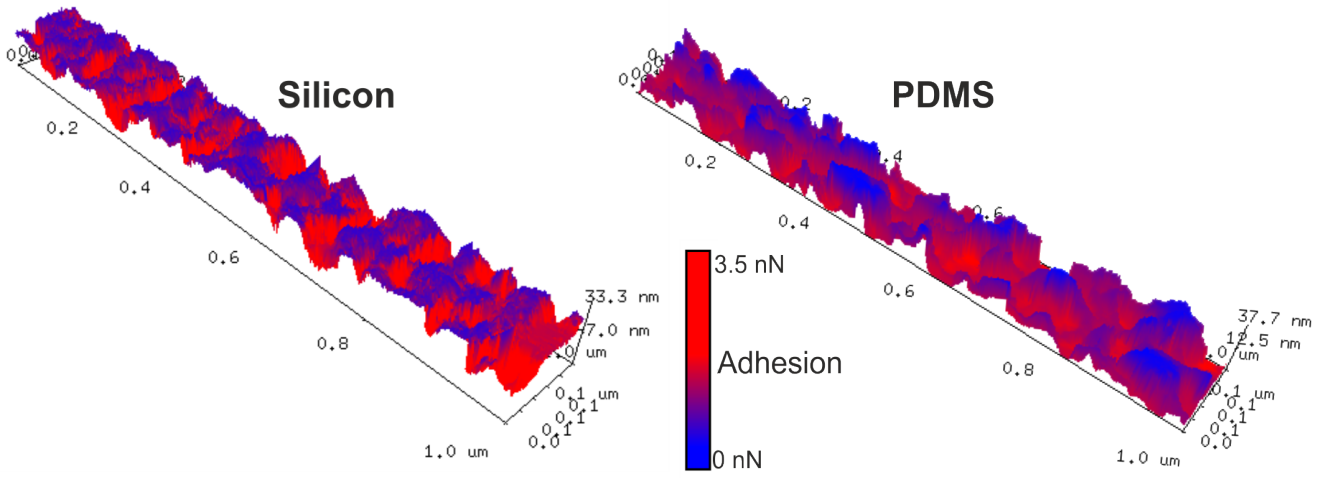

Fig. S2 Overlay of height data (geometry) and adhesion forces (color) between a hydrophobized tip and the surfaces of a silanized silicon and a PDMS surface with 7 nm RMS roughness. (Note, that the high aspect ratio tips needed to scan the rougher surfaces are not hydrophobic and, therefore, only the surface with the lowest RMS value was scanned as an example.)

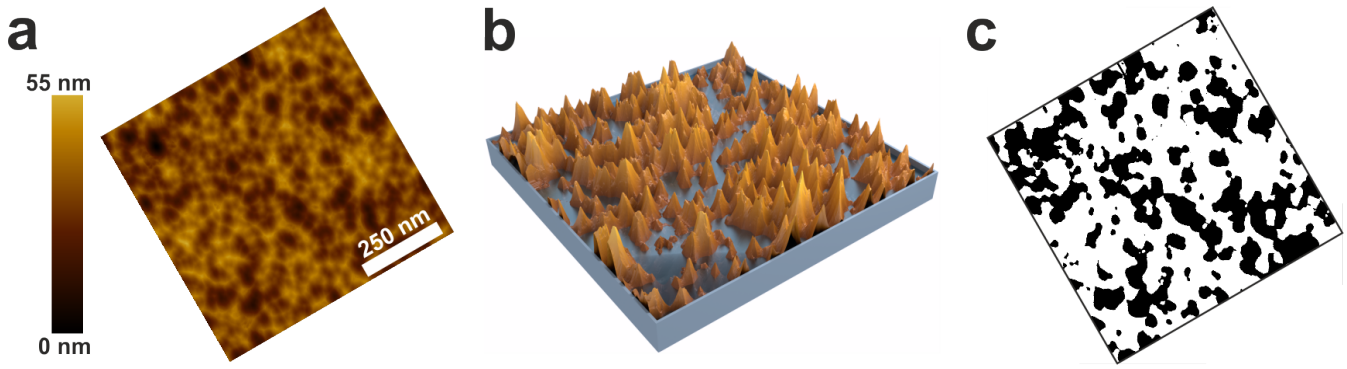

Fig. S3 a) Top view of a deconvoluted (and rotated) AFM image of the nanostructured surface. b) Three dimensional view of the surface from (a) 'filled' with water to a certain threshold height h_t. c) Corresponding black-and-white representation of the image from (a) and threshold height h_t.

Exemplary Visualization of the Minkowski Functionals

For the Minkowski analysis, the AFM images are converted to several different black-and-white images. This conversion is illustrated in Fig. S3 for one exemplary threshold height: the three dimensional structure of the surface is 'filled' from the bottom with water until a certain level (i. e. the threshold height) is reached. Then, each part of the surface above the water level is converted to white and each part below the water level to black, which results in the image shown in Fig. S3 c.

The way in which the Minkwoski measures are obtained from the black-and-white images is shown in Fig. S4 for three exemplary threshold heights: to obtain the Euler characteristic of a certain image, the number of white (black) unconnected regions of the image is counted positively (negatively), represented by the small numbers in Fig. S4 a. The second and third Minkowski measure are the perimeter of the black and the area of the white regions, as indicated by the red lines and green areas in Fig. S4 b and c. Performing this analysis for all threshold heights and plotting the three Minkowski measures in dependence of each threshold height, the graph shown in Fig. S4 d is obtained, which contains the complete additive shape information of the surface.

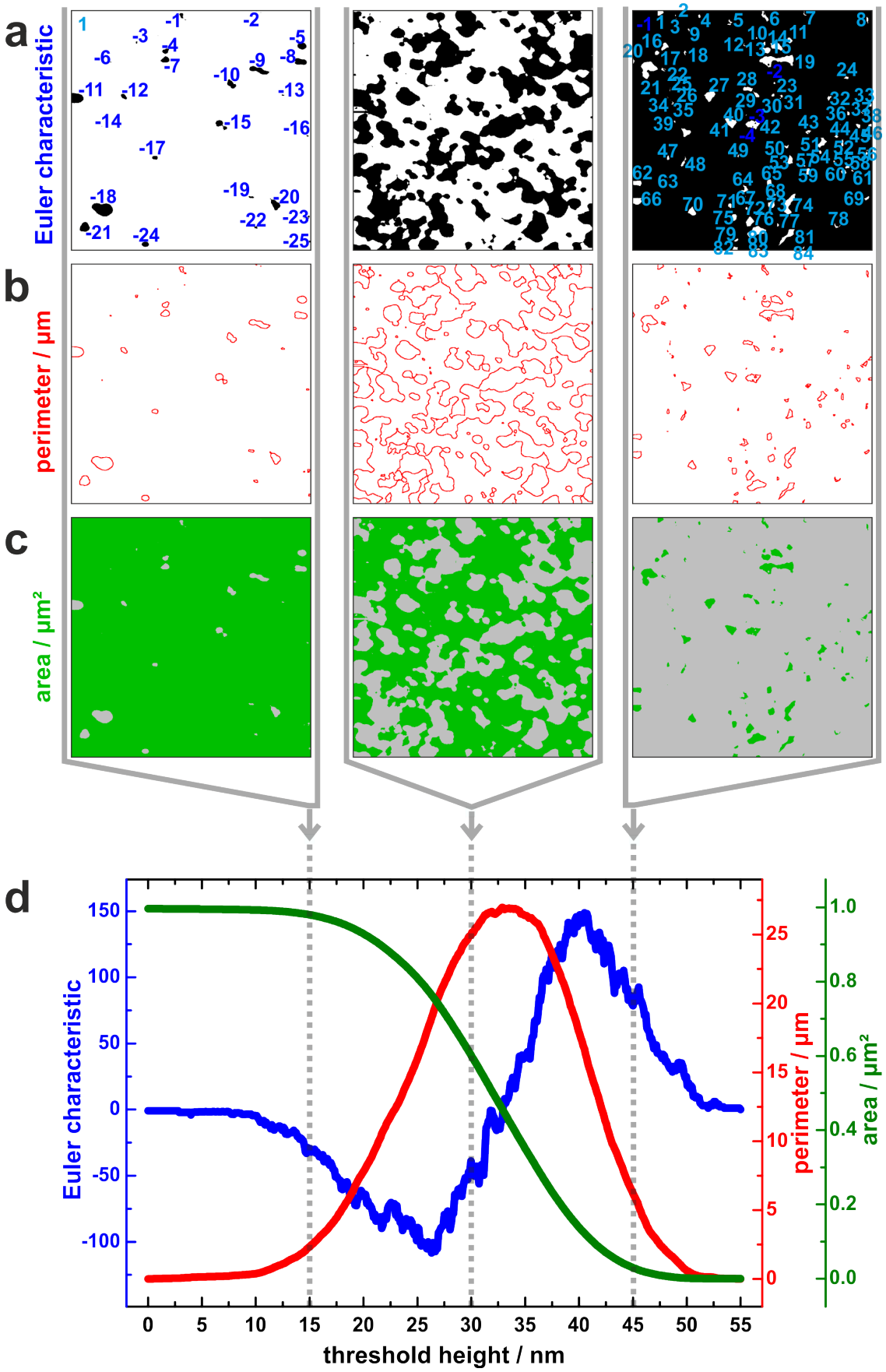

Fig. S4 Visualization of the Minkowski functionals for an AFM topography scan of an etched Si wafer (7 nm RMS roughness) for three different threshold heights (15 nm, 30 nm, 45 nm). (In the middle panel of the Euler characteristic, no numbers are given for reasons of clarity.)

Not Normalized Minkowski Functionals of the Nanostructured Surfaces

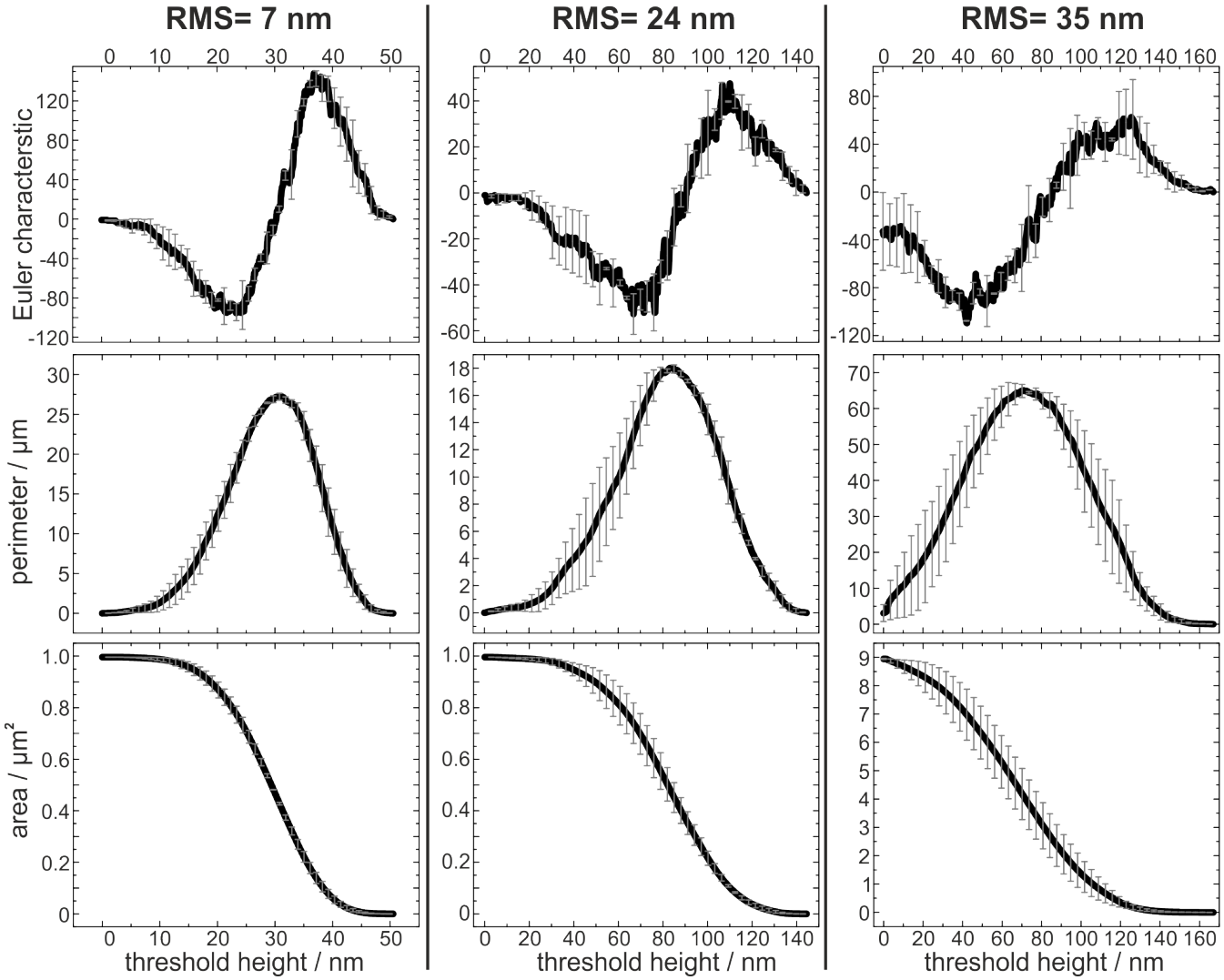

Fig. S5 Minkowski functionals in dependence of the threshold height for all surfaces (averaged over different surfaces of the same etching time). For the surfaces with RMS values of 7 nm and 24 nm the scan size was 1 μm^2 while it was 9 μm^2 for the surface with an RMS value of 35 nm.

Reason for the Force Trigger of 300 pN

The concept of this work is to study bacterial adhesion under conditions as close as possible to the natural situation where they adsorb and attach 'freely' from a planktonic state. Hence, the 'real energies' that drive bacteria to a surface are in the range of a few kT, i. e. it is our experimental setup to apply as low forces as possible by the AFM cantilever. 300 pN were used as the maximum force with which the cells were 'pressed' onto the surfaces since lower forces were not applicable in the used setup. The question arises at which applied force the bacterium deforms. In this case, the applied force must overcome the turgor pressure of the cell. In another study, we were exactly probing this and found that changes in turgor pressure of *S. aureus* (initiated by adding salt) were not detected using a maximum applied force of 1 000 pN, yet were observable at 5 000 pN[6,7]. To see changes of the contact area of the bacteria on smooth surfaces, one also must press relatively hard: as we were able to show on *S. aureus* in another study[6,8], using up to 3 000 pN, the contact area remains unchanged, and it needs at least 30 000 pN to see changes of the contact area radius of 10–20 %. In other words, to probe the influence of higher applied forces, these forces must be orders of magnitude higher and are far away from the situation 'as close as possible to nature', that we want to study. Moreover, probing the penetration depth using higher forces, is risky since the cell wall can rupture[7] and is therefore beyond the scope of the present study.

Not Normalized Adhesion Forces on Nanostructured Hydrophobic Silicon

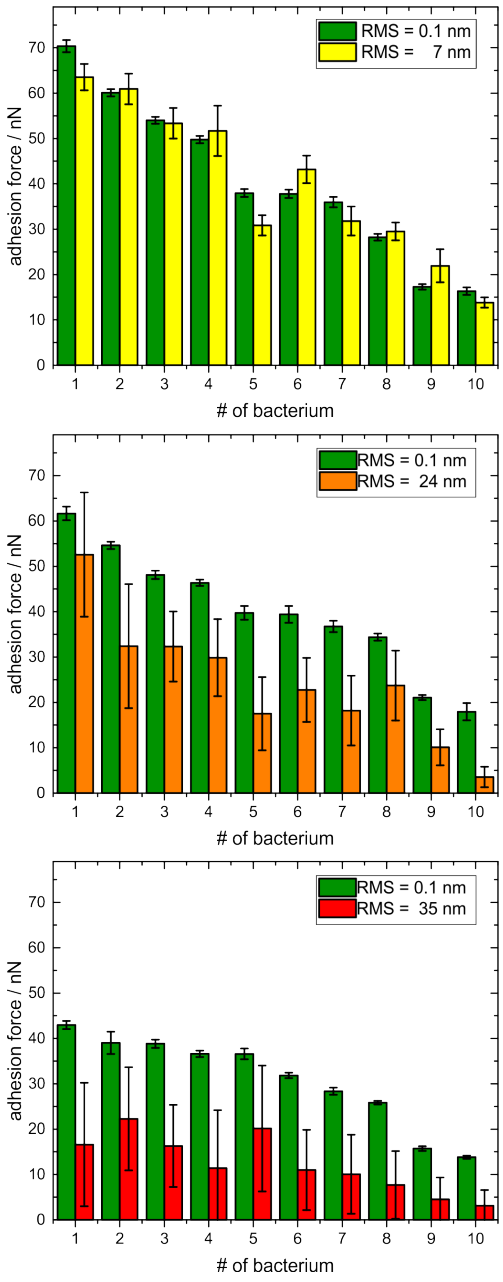

Fig. S6 Adhesion forces of 3×10 *S. aureus* cells to hydrophobic silicon of different roughness. With each cell, 200 force-distance curves were taken: first 50 force-distance curves on the smoothest surface, then 50 on one of the nanostructured surfaces, then again 50 curves on the smooth surface, and again 50 curve on the nanostructured surface. The forces on the smooth and nanostructured surfaces are shown as green and yellow/orange/red bars, respectively.

Tether Lengths of the Cells Used in Adhesion Experiments

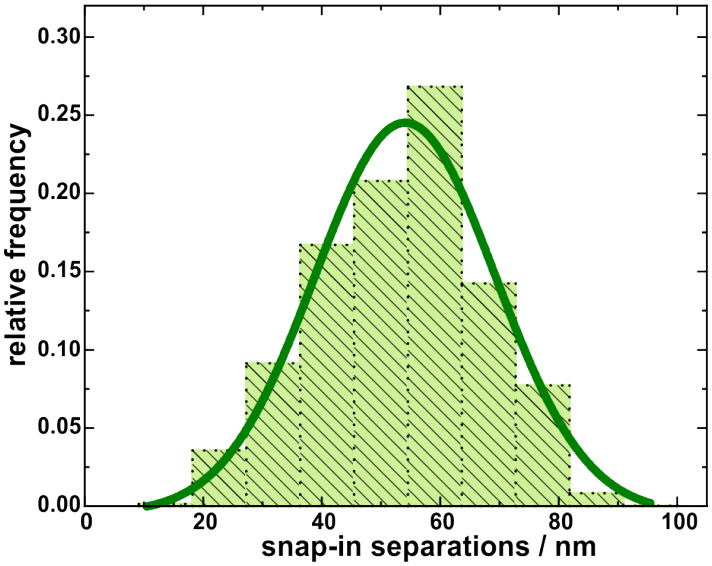

Fig. S7 Histogram (and Gaussian fit) of the snap-in separations determined from all force-distance curves of the adhesion measurements on the smooth hydrophobic silicon surface. The mean tether length of the 30 used cells is 53(3) nm. (The value in brackets gives the standard error of the mean.)

Correction of the 'Depth'-axis

For the x-axis in Fig. S8 (and the corresponding axis in Fig. 4 c in the main manuscript) the following must be considered: for all three substrates, the curves of the real surface area feature a 'flat' part at their beginning. For the surface with 7 nm RMS roughness, this part is very short (few nm) while it is rather long for the surface with 35 nm RMS roughness (several tens of nm). The reason for these flat parts of the curves is the fact that the top of all surfaces consist of very steep 'peaks'. The size and number of these peaks vary greatly for the different surfaces (e. g., the top 30 nm of the surface with 35 nm RMS roughness consist of 3 peaks/μm^2 while they consist of 57 peaks/μm^2 for the surface with 24 nm RMS roughness). Given the average radii of the contact area of *S. aureus* cells of about 150–300 nm[8], and since these peaks are distributed over the entire surface, an *S. aureus* cell approaching the substrate from above will not necessarily come in contact with these high structures, but only reaches the surface at lower height values. We call the average value of these heights 'mean surface top height' and have determined it numerically, as described in the next paragraph.

Thereto, we randomly positioned a large number of circles (here: 10,000) all with a radius of 250 nm (the average contact area radius for *S. aureus*[8]) on the images of the nanostructured surfaces and determined the height at which these circles first come into contact to the surface from above, i. e. the highest point inside each circle. The average of these values for all circles and each set of surfaces give the 'mean surface top height' for all sample sets. The distances of these heights from the absolute top heights are 34 nm, 6 nm and 2 nm for the surfaces with RMS roughnesses of 35 nm, 24 nm and 7 nm, respectively. Thus, the x-axis for each curve in Fig. S8 a can be corrected by shifting it in positive direction by the calculated distances. This way, we obtain the 'typical distance from top' for each surface (colored x-axes in Fig. S8). Instead of shifting the axes, also each data set can be shifted in negative x-direction by the corresponding mean surface top height (Fig. S8 b). Thereby, averaging the axis and shifting by the mean surface top height afterwards (as described above) gave the same curves as the inverse order, i. e. that for every circle mentioned above a curve with the corresponding x-axis was calculated and all these curves were averaged thereafter.

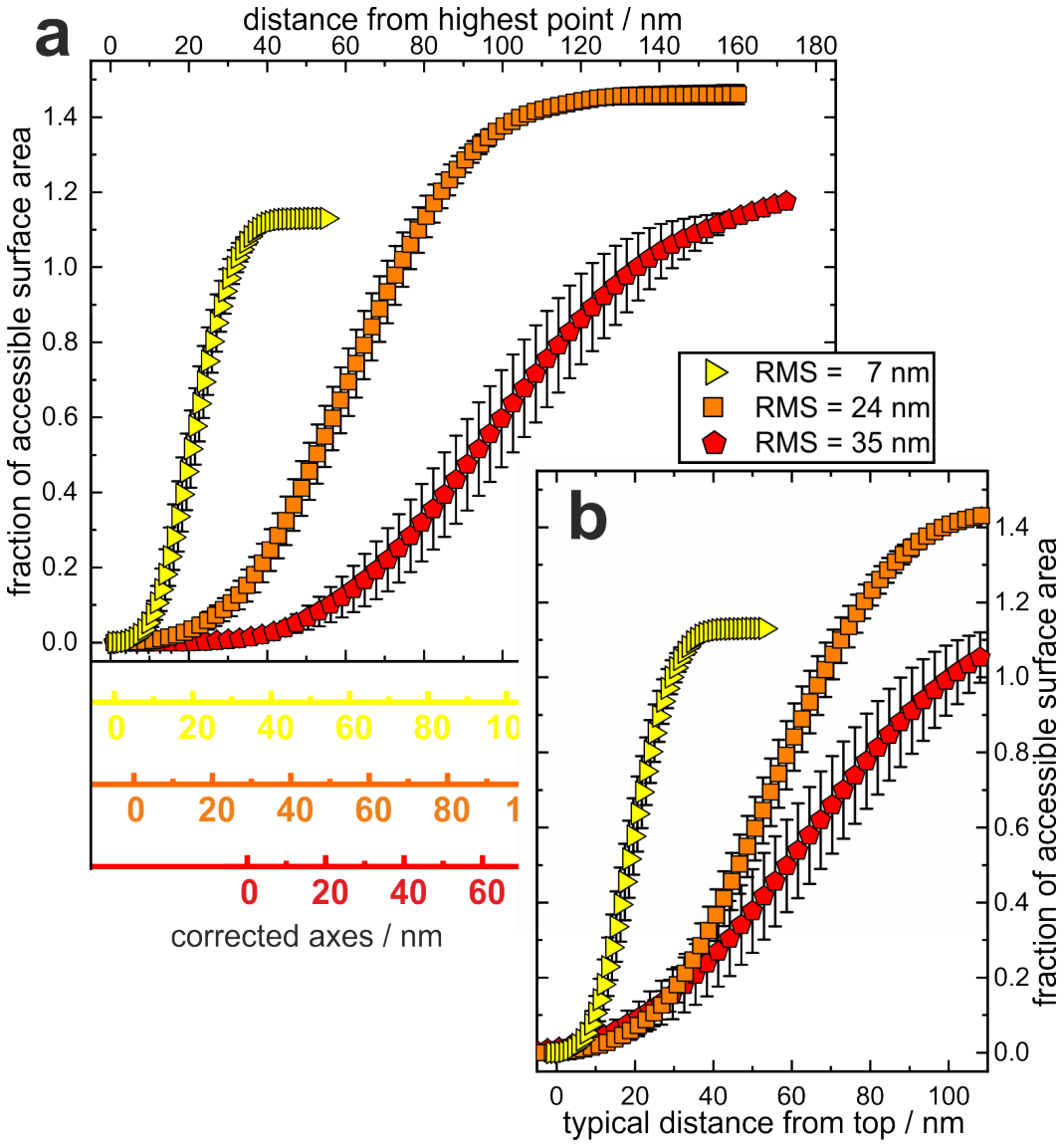

Fig. S8 Accessible fraction of surface area in dependence of the original and the corrected depth values from top of the surface (see text for details). In Fig. 4 c in the main manuscript, the axes are switched for illustrative purposes.

Adhesion of *Staphylococcus carnosus* to Nanostructured Silicon

Figure S9 shows the results of adhesion measurements of *Staphylococcus carnosus* (*S. carnosus*) on the nanostructured silicon surfaces: since this species is not clinical-relevant and experiments on a single-cell level are very time intensive, we did not reach the same large number of cells as for *S. aureus* that were used for the experiments in the manuscript, therefore the error bars are somewhat larger. Nevertheless, we see for *S. carnosus* the very same trend: since this species has a little shorter tether length of 43(2) nm (green rectangle in Fig. S9), also the mean adhesion forces are slightly smaller than for *S. aureus*, but they also fit the fraction of accessible surface area in a depth of 43 nm (vertical rectangles in Fig. S9).

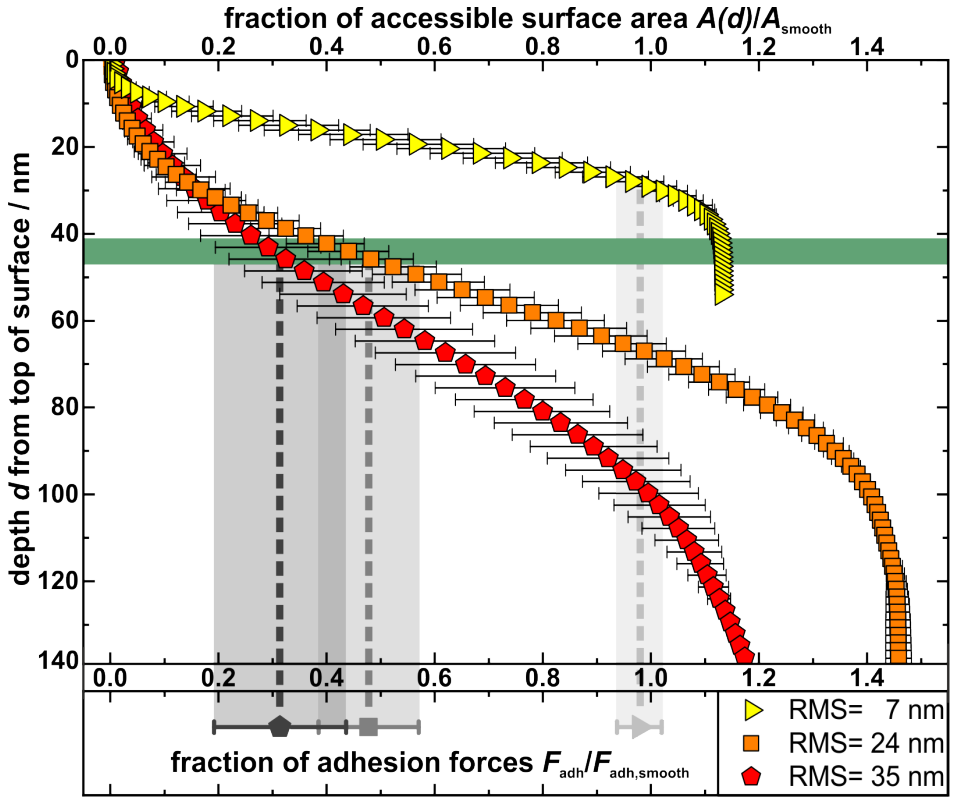

Fig. S9 Depth d from top of the surface and corresponding fraction of accessible surface area of all nanostructured substrates compared to the total surface area of a smooth substrate. The light-colored vertical rectangles show the relative decrease of adhesion forces on the nanostructured surfaces (The middle line of each rectangle indicates the mean value of adhesion forces and the width corresponds to the error of the mean.) The green horizontal rectangle indicates the mean tether length of the used *S. carnosus cells* which is 43(2) nm.

Adhesion of *Staphylococcus aureus* to Nanostructured PDMS

As a preliminary study of a different type of chemical homogenous surfaces, the hydrophobized silicon surfaces that were used for the experiments in the manuscript were filled with (liquid) non-crosslinked PDMS. After crosslinking (at 70 °C for 18 hours), the PDMS was gently peeled off (called mold casting). As it can be seen in the AFM images in Fig. S10 a, this procedure results in nanostructured surfaces. They were characterized by Minkowski functionals (see Fig. S10 b). Then, the adhesion forces of S. aureus cells to the nanostructured PDMS surfaces were measured as described in the manuscript. Results are shown in Fig. S10 c and confirm our results on nanostructured silicon surfaces: for the surface with the lowest and the medium RMS value, the average adhesion forces (having larger error bars) are again in good agreement with the accessible surface area in a depth of 50 nm. For the surface with the highest RMS value, we find slightly stronger adhesion than it would be expected by the total surface area. This cannot be studied in detail at this stage, but is very likely an effect of the higher elasticity of PDMS compared to the silicon surfaces, which leads to an enhanced contact area between cell and substrate[5,9,10]. Under this assumption, the direction of the shift in adhesion forces (forces higher than expected) can be explained qualitatively: since the cell is pressed onto each surface with the same force, the pressure is higher where the cell–surface contact is smaller, namely on the surface with the highest RMS value.

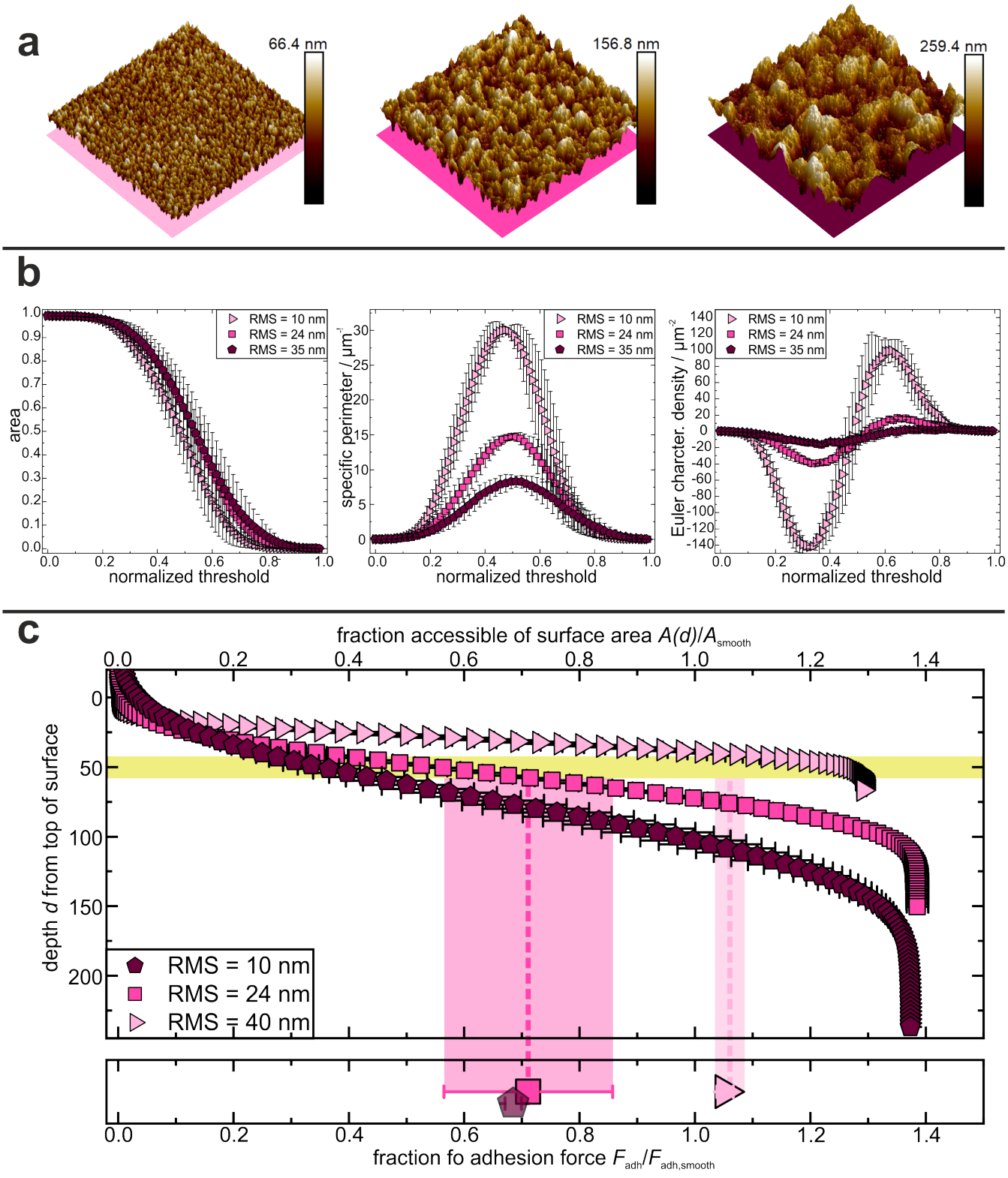

Fig. S10 a) AFM scans of nanostructured PDMS ($3 \times 3\ \mu m^2$), b) Normalized Minkowski functionals of nanostructured PDMS surfaces, c) Fraction of bacterial adhesion forces compared to fraction of accessible surface area in a depth of 50 nm.

References

1 P. Loskill, H. Hähl, T. Faidt, S. Grandthyll, F. Müller and K. Jacobs, *Adv. Colloid Interface Sci.*, 2012, **179**, 107–113.
2 P. Loskill, H. Hähl, N. Thewes, C. T. Kreis, M. Bischoff, M. Herrmann and K. Jacobs, *Langmuir*, 2012, **28**, 7242–7248.
3 M. Lessel, O. Bäumchen, M. Klos, H. Hähl, R. Fetzer, M. Paulus, R. Seemann and K. Jacobs, *Surf. Interface Anal.*, 2015, **47**, 557–564.
4 D. Quéré, *Physica A: Statistical Mechanics and its Applications*, 2002, **313**, 32–46.
5 A. L. Weisenhorn, M. Khorsandi, S. Kasas, V. Gotzos and H.-J. Butt, *Nanotechnology*, 1993, **4**, 106.
6 P. Loskill, P. M. Pereira, P. Jung, M. Bischoff, M. Herrmann, M. G. Pinho and K. Jacobs, *Biophys. J.*, 2014, **107**, 1082–1089.
7 S. Pogodin, J. Hasan, V. A. Baulin, H. K. Webb and V. K. Truong, *Biophys. J.*, 2013, **104**, 835–840.
8 C. Spengler, N. Thewes, P. Jung, M. Bischoff and K. Jacobs, *Nanoscale*, 2017, **9**, 10084–10093.
9 K. Johnson, *Tribology International*, 1998, **31**, 413–418.
10 B. N. Persson, O. Albohr, U. Tartaglino, A. Volokitin and E. Tosatti, *Journal of Physics: Condensed Matter*, 2004, **17**, R1.